LUNAR FLOOR-FRACTURED CRATERS: INTRUSION EMPLACEMENT AND ASSOCIATED GRAVITY ANOMALIES. L. M. Jozwiak[1], J. W. Head[1], R. J. Phillips[2], M. T. Zuber[3], D. E. Smith[3], G. A. Neumann[4], D. M. H. Baker[1], L. Wilson[5], and C. Thomason[2]. [1]Department of Geological Sciences, Brown University, Providence, RI 02912. [2]Southwest Research Institute, Boulder, Colorado 80302. [3]Department of Earth, Atmospheric, and Planetary Science, Massachusetts Institute of Technology, Cambridge, MA 02142. [4]Solar System Exploration Division, NASA Goddard Space Flight Center, Greenbelt, MD 20768. [5]Environmental Science Department, Lancaster University, Lancaster LA1 4YQ UK. Corresponding Author: lauren_jozwiak@brown.edu

Introduction: Floor-fractured craters (FFCs) are a class of lunar crater characterized by anomalously shallow, fractured floors, with additional characteristics including moats, dark halo deposits, and patches of mare material [1,2]. The two proposed formation mechanisms for floor-fractured craters include viscous relaxation [e.g. 3] and magmatic intrusion and sill emplacement [1]. Recent morphologic analysis using Lunar Orbiter Laser Altimeter (LOLA) data and Lunar Reconnaissance Orbiter Camera (LROC) images supports magmatic intrusion and sill formation as the formation mechanism of floor-fractured craters [2].

Using this result, we examine the volcanic features associated with floor-fractured craters, with emphasis on their relationship to the evolution of the magmatic intrusion. We also use Gravity Recovery and Interior Laboratory (GRAIL) data to investigate the Bouguer gravity anomalies associated with floor-fractured craters.

Intrusion Emplacement: The intrusion of a magmatic body beneath overlying strata (such as a crater floor) produces initial deformation and observable surface morphologies [4, 5]. The end-member intrusion morphologies, sill and laccolith, are shown schematically in Figure 1. The emplacement stage encompasses processes associated with the dike propogation, sill/laccolith formation and inflation, and subsequent fracturing and deformation of the surrounding and overlying rock. The sill and laccolith end-member morphologies have been interpreted from morphologic evidence [2,6], and are consistent with modeled end-member morphologies for the intrusion of a magmatic body beneath a crater floor [7]. *Thorey and* Michaut [7] establish a critical relationship for determining the end-member intrusion morphology between the depth of the intrusion and the diameter of the intrusion. An analysis of FFC surface morphology suggests that craters with $D < 40$ km possess domed floors indicative of a laccolith intrusion morphology; FFCs with $D > 40$ km possess flatter floors and a more sill-like intrusion morphology. Thus we conclude that the intrusion diameter is the more important parameter in determining final intrusion morphology. Measurements of intrusion thickness (method from [2]) suggest an average intrusion thicknes of 1 km, and using a Stefan cooling solution, we determine that a 1 km thick intrusion would take 4 years to solidify (that is, reach the solidus, not necessarily equilibrium with the country rock).

Coincident with the intrusion emplacement, is the process of magma degassing, involving both initial magma volatiles, such as H_2O [8], and the in situ production of CO [9,10]. How these volatiles evolve during intrusion emplacement, and particularly how they interact with fractures formed during intrusion emplacement has important bearing on what (if any) volcanic surface features are formed.

Volcanic Features: The surface volcanic features associated with floor-fractured crater intrusion evolution (Figure 1) are categorized as 1) vents, with or without associated dark mantling material, Figure 2a; 2) dark halo deposits representing pyroclastic material, generally surrounding a vent, Figure 2b; 3) surface lava flows located primarily at the crater floor-wall interface, Figure 2c. There is likely a close relationship between volcanic features and floor fractures, for example transport of magma along faults at the intrusion periphery could lead to the observed surface flows (Figure 2c). *Jackson and Pollard* [1988] show a relationship between fracture location (over areas of greatest bending) and small accessory dike fed from the main intrusion. Thus, we conclude that the volcanic features associated with floor-fractured craters are related to either volatile release of magma localized beneath fractures, or physical transport of magma along these fractures and onto the crater floor.

We postulate that vents are the result of passive volatile leaking and degassing resulting in collapse of the overlying material. This would be promoted by low-pressure foams (~5 MPa) that collapse [11, 12]. Dark mantling deposits can be the result of vulcanian eruptions [13] that possess a pressure in excess of ~ 15 MPa [11, 14, 15] sufficient to both fracture the overlying rock and disperse pyroclastic material around the central vent. Patches of mare material represent lava flows sourced from the intrusion, and formed by the transport of magma along fractures related to the uplift of the crater floor.

Gravity Structure: Impact craters on both the Earth and the Moon possess a negative Bouguer anomaly [16, 17] which is commonly attributed to the brecciated region beneath the crater floor [17]. Floor-fractured craters formed by a subcrater magmatic intrusion would possess a high-density component in addition to the low-density breccia component. This intrusion contribution may manifest as a positive Bouguer anomaly for the crater floor as a whole, or perhaps as a less negative Bouguer anomaly than would be predicted. We note that on the Moon, craters with diameter greater than ~150 km display positive Bouguer anomalies, which has been attributed to mantle uplift [18]. Using GRAIL data GRGM720B model, we analyze the Bouguer anomaly associated with all catalogued floor-fractured craters [2]. We observe three categories of gravity anomaly: 1) mascon dominated, 2) null signal, 3) positive center [19]. The Bouguer anomaly associated with craters that are located within lunar basins or close to the edge of basins is often overpowered by the Bouguer anomaly of the basin leading to the mascon dominated group. The second group, null signal, is ascribed to craters with a Bouguer anomaly indistinguishable from the surrounding region. These craters have diameters 20-40 km, and given the model spatial block size (~10 km) it is possible that the crater floor Bouguer anomaly signal is convolved with and obscured by the regional crater Bouguer anomaly. Positive center craters have a positive Bouguer anomaly for the crater floor region. Figure 3 shows the Bouguer anomaly of the crater Vitello, including a plot of incremental topography and Bouguer anomaly showing an inverse relationship between the crater topography and the strength of the Bouguer anomaly. Of the 88 floor-fractured craters that were not mascon dominated 71 display positive Bouguer anomalies [6].

Conclusions: Floor-fractured craters are a class of lunar craters postulated to form as a result of magmatic intrusion and sill formation [1, 2]. The evolution of these intrusions can lead to volcanic features such as vents, pyroclastic deposits, and lava flows. These features are spatially correlated with the floor-fractures and their formation is dependent on the pressure generated by exsolved volatiles in the magma transported along peripheral fractures. In general, impact craters possess negative Bouguer anomalies [16, 17]; however craters hosting a magmatic intrusion should possess a positive Bouguer anomaly reflecting this high-density component. Analysis of GRAIL data shows that 71 of 88 applicable floor-fractured craters host a positive Bouguer anomaly, further supporting the magmatic intrusion and sill formation hypothesis.

References: [1] Schultz, P. H. (1976) *The Moon, 15*, 241-273. [2] Jozwiak L. M. et al. (2012) *JGR, 117*, E11. [3] Hall, L. et al. (1981) *JGR, 86*, 9537-9552. [4] Pollard, D. D. and Johnson, A.M. (1973) *Tectonophysics, 18*, 311-354. [5] Jackson, M. D., and Pollard, D. D. (1988) *GSA Bulletin, 100*, 117-139. [6] Jozwiak, L. M., et al. (2013) *Manuscript in prep*. [7] Thorey, C. and Michaut, C. (2013) *LPSC XLIV*. Abstract # 1508. [8] Saal, A. E. et al. (2008) *Nature, 454*, 192-196. [9] Sato, M. (1979) *Proc. LPS X*, 311-325. [10] Fogel, R. A., and Rutherford, M. J. (1995) *Geochem. Et Cosmochim. Acta, 59*, 201-225. [11] Head, J. W. et al. (2002) *JGR, 107*, E1. [12] Jaupert, C., and Vergniolle, S. (1989) *J. Fluid Mech., 203*, 347-380. [13] Head, J. W., and Wilson, L. (1979) *Proc. LPS X*, 525-527. [14] Touloukian, Y. S., et al. (1980) *Physical Properties of Rocks and Minerals*. McGraw-Hill, New York. [15] Tait, S., et al. (1989) *EPSL, 92*, 107-123. [16] Dvorak, J. J., and Phillips, R. J. (1977) *GRL, 4*, 380-382. [17] Pilkington, M. and Grieve, R. A. F., (1992) *Rev. of Geophys., 30*, 161-181. [18] Baker, D. M. H., et al. (2013) *LPSC XLIV*. Abstract #2662. [19] Jozwiak, L. M., et al. (2013) *NLSI LSF 2013*.

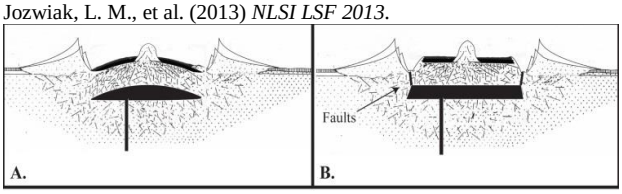

Figure 1: Schematic cross-sections of end-member floor-fractured crater intrusions. A) Laccolith style intrusion which produces a domed crater floor. B) Slab-like sill intrusion which results in piston-like uplift of the crater floor, aided by large peripheral faults.

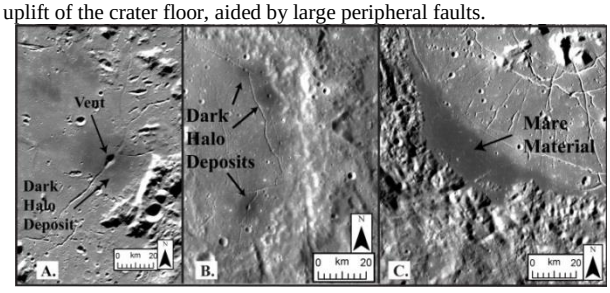

Figure 2: LROC-WAC images of volcanic features associated with floor-fractured craters. A) Large vent from the NE part of the crater floor of Schrödinger crater. B) Pyroclastic dark mantling deposits located in the eastern part of crater Alphonsus. C) Lava flows along the edge of the floor in crater Humboldt. Note in all cases the volcanic feature is located on a fracture.

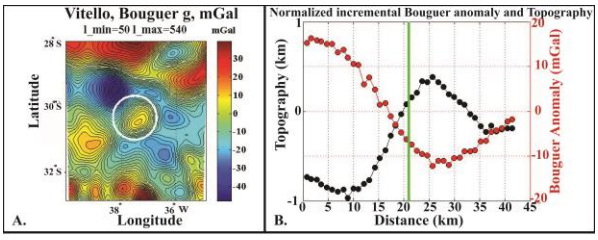

Figure 3: Bouguer gravity anomaly for the crater Vitello, D = 44 km. There is a positive Bouguer anomaly in the center of the crater floor (A), which underlies a region of strong concentric fractures and uplift on the crater floor itself. B) Incremental topography (LOLA) and Bouguer anomaly shown in radial distance from the crater center.